ARTICLE

An enhanced fluorescent ZIF-8 film by capturing guest molecules for light-emitting applications

Qiufeng Liu,[a] Shouqin Tian,*[a] Xiujian Zhao [a] and Gopinathan Sankar [b]

Received 00th January 20xx,
Accepted 00th January 20xx

DOI: 10.1039/x0xx00000x

Metal organic frameworks (MOFs) constructed by metal ions/clusters and organic linkers become new porous luminescent materials and thus have attracted much attention. But their photoluminescence quantum yield (PLQY) is not high and the photoluminescence mechanism is still unclear. In order to solve the problem, zeolitic imidazolate framework-8 (ZIF-8, a kind of MOFs) composite films containing small molecules acetic acid were successfully prepared on glass substrate by sol-gel method and exhibited a high PLQY of 54.42% in this work. Compared with pure ZIF-8 film, the obtained ZIF-8 composite film presented a significant enhancement in the blue light emission. Moreover, PLQY of the ZIF-8 composite film can be controlled to a certain extent by adjusting the mole ratio of the ligands to the zinc source. Among them, the ZIF-8 film prepared at the mole ratio of 2.5:1 showed higher transmittance and the fluorescence quantum efficiency was up to 54.42%, which may be attributed to the electron transfer between acetic acid as electron-donor and ZIF-8 structure caused by their relatively strong hydrogen bonding interaction. This work may provide a new insight into the enhanced fluorescence of MOFs materials for light-emitting applications.

1. Introduction

Recent years, photoluminescent materials have attracted much attention facing the global problem of environmental contamination and limited energy resources, which play an important role in the performance of solar energy conversion for light-emitting applications. In this sense, many works have been focused on these materials possessing excellent photoluminescence performance like quantum dots,[1,2] perovskites,[3,4] or some 2D nanomaterials.[5] Those luminescent materials are showing high fluorescence quantum efficiency and tunable luminescence over a wide energy range. However, some intrinsic defects such as easy oxidation, aggregation-caused fluorescence quenching and poor luminescence stability would have a great influence on optical applications.[6]

Luminescent metal organic frameworks (LMOFs) constructed by metal ions/clusters and organic linkers are new porous luminescent materials with high pore volumes, large specific surface areas and structure designability, showing various and tunable optical properties for light emitting applications.[7] Both metal ions/clusters and ligands can serve as chromophore to generate luminescence. In this sense, different luminescent MOFs materials can be prepared by the selection of metal ions/clusters and ligands and the structural design. Zeolitic imidazolate frameworks (ZIFs) as a class of MOFs composed of metal ions/clusters and imidazolate ligands are promising materials, possessing exceptional thermal and chemical stability and size controlling design.[8,9] Zeolitic imidazolate framework-8 (ZIF-8) is a typical representative of ZIFs having attracted intense interests due to its large pores (11.6 Å) and higher surface area (1630 m^2/g), which is comprised of Zn ions interconnected with 2-methylimidazolate (Hmim) ligands to form the sodalite (SOD) zeolite-like structure.[10] Since the luminescence of ZIF-8 is linker-based, the low luminescence activity limits its luminescence applications. In this sense, many methods have been tried to improve the luminescence properties through encapsulating or directly forming composite materials. On the one hand, introducing luminescent materials like carbon quantum dots,[11,12] tris(8-hydroxyquinoline)-aluminium,[13] lanthanide complexes[14,15] into ZIF-8 to form core-shell structurers or directly forming composite materials to improve optical performance.[16,17] On the other hand, small molecules such as dimethylformamide (DMF) in ZIF-8 are used for tuning electron density distribution to form white-light emitting.[18] To a certain extent, the luminescent properties and stability of these fluorescent materials have been improved, but there is still large room for optimization of optical performance such as photoluminescence quantum yield. In addition, the photoluminescence mechanism of ZIF-8 is still unclear. Therefore, it is great necessary to improve PLQY of ZIF-8 and reveal its photoluminescence mechanism.

In this paper, considering the low blue light emission of ZIF-8, here we successfully synthesized a blue light enhanced fluorescent ZIF-8 film through sol-gel method by introducing

[a] State Key Laboratory of Silicate Materials for Architectures, Wuhan University of Technology (WUT), No. 122, Luoshi Road, Wuhan 430070, P. R. China, E-mail address: tiansq@whut.edu.cn (S. Tian).
[b] Department of Chemistry, Materials Chemistry Centre, University College London, 20 Gordon St., London WC1H 0AJ, UK.

†Electronic Supplementary Information (ESI) available: [details of any supplementary information available should be included here]. See DOI: 10.1039/x0xx00000x

guest molecules (CH_3COOH) to form relatively strong hydrogen bonding interaction between acetic acid and ZIF-8 which can lead to an easier electron transfer for enhanced photoluminescence performance. And the relative content of guest molecules in the obtained ZIF-8 film can be controlled by adjusting the mole ratio of the ligands to zinc salt and the solidifying temperature, and puts important effects on the structure and properties of ZIF-8 films, which will be investigated in detail. This work may provide a new insight for ZIF-8 film with enhanced fluorescence in light-emitting applications.

2. Experimental

2.1 Materials

Zinc acetate dihydrate ($Zn(CH_3COO)_2{\cdot}2H_2O$, ≥99.0%, Shanghai China), 2-methylimidazole ($C_4H_6N_2$, 99%, sigma-aldrich), methanol (≥99.5%, Shanghai China), ethanol (≥99.7%, Shanghai China), acetone, all chemicals were used without further purification, and the deionized water was obtained through the purified water system in our lab.

2.2 Preparation of ZIF-8 films

A series of ZIF-8 films were synthesized by the following steps shown in Fig. S1. Firstly, $Zn(CH_3COO)_2{\cdot}2H_2O$ (0.005 mol) and Hmim (0.0125 mol) were mixed in 1 mL methanol, and then stirring at room temperature to form transparent ZIF-8 precursor sol. Afterwards, quartz glass substrates were washed using ultrasonic cleaning machine with solvents of acetone, deionized water and ethanol for 40 minutes in turn. ZIF-8 sol was coated on clean quartz glasses through spin-coating method to obtain the ZIF-8 wet film. Next, the ZIF-8 film was obtained by solidifying at 100 ˚C for 10 h. And keeping the concentration of $Zn(CH_3COO)_2{\cdot}2H_2O$ at 5 mol/L in ZIF-8 sol and adjusting the amount of Hmim, a series of ZIF-8 films were synthesized with different Hmim/$Zn(CH_3COO)_2{\cdot}2H_2O$ mole ratios (2.5:1, 3:1, 3.5:1, 4:1, 5:1, 6:1 and 8:1) using the same steps above.

2.3 Characterizations

The phase structure of synthesized films was characterized by a X-ray diffraction (XRD, Empyrean, Netherlands) using grazing incidence scanning with a Cu Kα radiation (λ = 1.5418 Å) at a scanning rate of 0.02° 2θ s^{-1}. The morphology and thickness of obtained films were performed on German Zeiss Ultra Plus field-emission scanning electron microscopy (FESEM). The Fourier transform infrared spectra were recorded on a Fourier transform infrared spectrometer (FTIR, Nicolet6700, USA) in the spectral range 4000-400 cm^{-1} for detecting functional groups in the films. The integrated thermal analysis system (TG-DSC-MS, STA449F3, NETZSCH, Germany) was employed to detect samples' thermal response to temperature and changes of components. The electronic structures and surface compositions of the films were determined by an X-ray photoelectron spectrometer (XPS, ESCALAB 250Xi, USA) accompanied with the function of ultraviolet photoelectron spectroscopy (UPS). The UV-vis absorption spectra were obtained using a UV-vis spectrophotometer (UV-1600). And photoluminescence spectra (PL) were measured at room temperature with a fluorescence spectrophotometer (QM/TM/NIR, USA). The PL quantum efficiency was measured using a UV-NIR absolute PLQY spectrometer (Quantaurus-QY Plus, Hamamatsu, Japan). The fluorescence lifetime decay curves of films were obtained by a time-resolved fluorescence spectrometer (Newport, USA) using the time-correlated single photon counting (TCSPC) technology, and excitation light is pumped by the femtosecond laser (Spirit 1040-8W, Spectra-Physics, USA).

3. Results and discussion

3.1 Characterizations

Fig. 1 shows the XRD patterns of the ZIF-8 films synthesized with different mole ratios of Hmim/$Zn(CH_3COO)_2{\cdot}2H_2O$ on quartz glasses. All diffraction peaks of the films can be indexed to ZIF-8 according to the literature reports about ZIF-8.[19-21] Differently, it can also be seen that there is a strong broad peak package at the range of 10° to 20° among films synthesized with the mole ratios between 2.5:1 and 4:1, which may be attributed to the amorphous ZIF-8 structure. However, films synthesized at high mole ratios (5:1, 6:1 and 8:1) show high crystallized ZIF-8 structures. This may be related to the chemical environment in which ZIF-8 films were synthesized, and this will be discussed later.

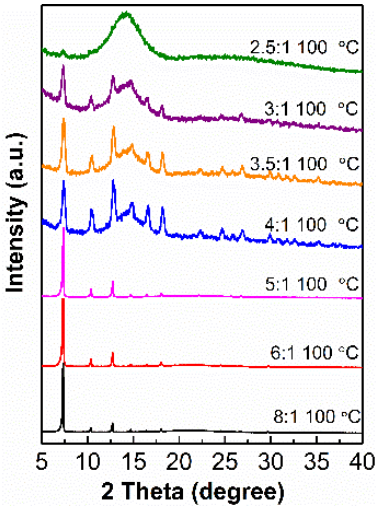

Fig. 1. XRD patterns of ZIF-8 films synthesized with different mole ratios of Hmim to $Zn(CH_3COO)_2{\cdot}2H_2O$.

In order to characterize the morphology and structure of the obtained ZIF-8 films synthesized with different mole ratios of reactants, FESEM measurements were employed and the results are shown in Fig. 2 and Fig. 3. It can be seen from Fig.2a and 2b, the surface of the ZIF-8 film synthesized with mole ratio of 2.5:1 is very smooth and continuous. However, the cross section of the film is uneven, this is consistent with the amorphous ZIF-8 structure in Fig. 1. Furthermore, small particles gradually appear on the surface of ZIF-8 films with the

increase of the mole ratio, as shown in Fig. 2e and 2g, eventually forming the typical rhombic dodecahedron of ZIF-8 structure[22-23] shown in Fig. 3. The possible reason for this phenomenon is related to the coordination degree between Hmim ligand and zinc salt at different mole ratios.

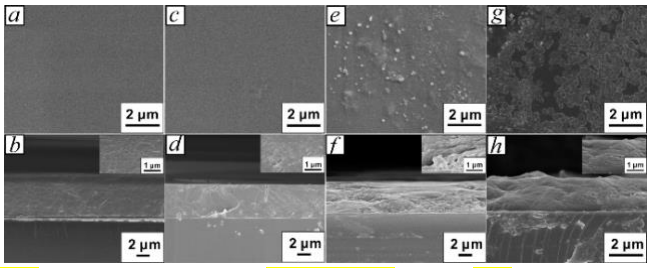

Fig. 2. FESEM images of ZIF-8 films synthesized with different mole ratios: 2.5:1 (a, b), 3:1 (c, d), 3.5:1 (e, f) and 4:1(g, h) for the surfaces (a, c, e, g) and the cross-sections (b, d, f, h), respectively.

To further investigate the reason for the formation of the ZIF-8 films about morphological and structural differences, FTIR characterizations were performed. As reported earlier, ZIF-8 structure is formed by the coordination of Zn^{2+} and organic ligands Hmim without any other guest molecules. The results of ZIF-8 sample synthesized with the mole ratio of 8:1 with high crystallization were shown in Fig. S2 and Table S1. The absorption peak at 422 cm^{-1} is attributed to Zn-N stretching vibration, and the peak at 1586 cm^{-1} is the stretching vibration of C=N. The peaks at 3137 cm^{-1} and 2932 cm^{-1} correspond to the C-H bond in the imidazole ring and in methyl group, respectively. The peaks at 1147 cm^{-1} and 995 cm^{-1} are the stretching vibration peaks of C-N. Furthermore, abroad peak between 3500 and 3200 cm^{-1} is the stretching of N-H bonds due to protonated imidazole.[24-27] This proves that ZIF-8 has been successfully formed by the coordination of zinc ions with Hmim linker. However, other samples of synthesized ZIF-8 films not only have the similar structure, but also exhibit a little difference shown in Fig. 4. Obviously, there is a broad peak which the wavenumber range is between 2400 and 3600 cm^{-1} shown in Fig. 4I, corresponding to stretching vibration of O-H[28] due to the forming of hydrogen bonds, especially in ZIF-8 films synthesized with low mole ratios of reactants (2.5:1, 3:1, 3.5:1 and 4:1). However, the stretching vibration of N-H due to protonated imidazole exists in all ZIF-8 films. And in Fig. 4II, the relative strength of the peak between 1500 and 1700 cm^{-1} increases with the decrease of the mole ratio. The possible reason is that small molecules CH_3COOH exist at low mole ratios and the stretching vibration peak of C=O in CH_3COOH overlaps with the stretching vibration peak of C=N. Furthermore, three peaks ascribed to the O-C=O in-plane bending vibration between 600 and 700 cm^{-1} can also be seen in ZIF-8 samples prepared with low mole ratios (in Fig. 4III).[29] However, the characteristic infrared vibration of acetic acid molecules is not obvious at high mole ratios (5:1, 6:1 and 8:1). These have been proved that ZIF-8 films with small molecules CH_3COOH may be formed at the low mole ratios (x is the ratio of the reactants Hmim to $Zn(CH_3COO)_2{\cdot}2H_2O$, $2.5 \le x \le 4$) while guest molecules barely exist in ZIF-8 structure at high mole ratios ($x \ge 5$). Additionally, these ZIF-8 samples of low mole ratios were picked out to heat treatment at 130 °C for 5 h and FTIR spectra were also measured for comparison shown in Fig. S3. It can be seen that the ZIF-8 films after heat treatment still maintain the structure of ZIF-8, but the wide absorption band (hydrogen bonds formed between ZIF-8 and acetic acid molecules) with the wavenumber in the range of 2400 to 3600 cm^{-1} is relatively reduced. In this sense, it reveals that the thermal stability of ZIF-8 and the presence of guest molecules (CH_3COOH) in ZIF-8 films at low mole ratios.

In order to accurately prove the composition of guest molecules, TG-DSC-MS characterizations in Ar/N_2 atmosphere were employed to detect possible guest molecules. The results are shown in Fig. S4-S10 for ZIF-8 films synthesized with different mole ratios

As seen from Fig. S4, the ZIF-8 film synthesized with the mole ratio of 2.5:1 releases its free guest molecules in the temperature range of 50 °C to 300 °C. And then the ZIF-8 structure begins to decompose above 300 °C. This is related to the thermal stability of ZIF-8,[30] which is consistent with the FTIR data from the aforementioned low-temperature heat treatment of ZIF-8 in Fig. S3. The traced guest molecules curves show that an obvious peak (M=60, CH_3COOH) is located at 196 °C. However, other traced guest molecules (M=18, H_2O; M=32, CH_3OH; M=82, Hmim) curves don't exhibit obvious peaks, and similar peaks of acetic acid are also observed in ZIF-8 films synthesized with other low mole ratios (Fig. S5-S7). This suggests that only acetic acid molecules exist in these ZIF-8 films. The weight losses of the ZIF-8 films synthesized with low mole ratios of 2.5:1, 3:1, 3.5:1 and 4:1 below 300 °C are ~20.26%, 17.05%, 15.34%, 16.53%,respectively. However, the peaks of acetic acid and other small molecules in the ZIF-8 films prepared with 5:1, 6:1 and 8:1 shown in Fig. S8-S10 isn't appeared. And the weight losses below 300 °C are 2.81%, 0%, 0%,respectively. This indicates that there are almost no guest molecules in ZIF-8 films synthesized at high mole ratios.

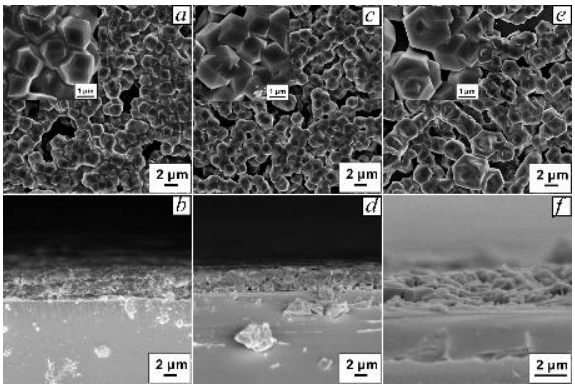

Fig. 3. FESEM images of ZIF-8 films synthesized with different mole ratios of reactants: 5:1 (a, b), 6:1 (c, d) and 8:1 (e, f) for the surfaces (a, c, e) and the cross-sections (b, d, f), respectively.

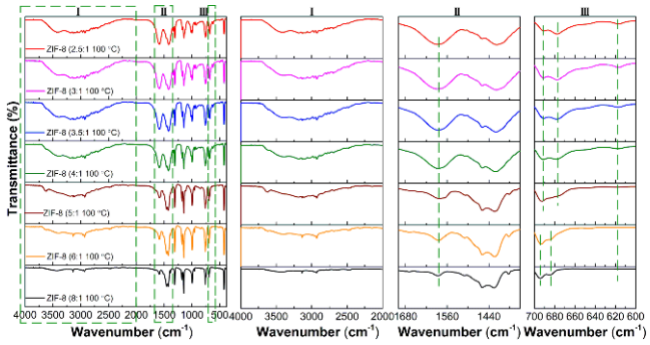

Fig. 4. FTIR spectra of ZIF-8 films synthesized with different mole ratios of reactants and the enlarged IR spectra (I-III) in the regions from 4000 to 2000 cm^{-1}, from 1700 to 1350 cm^{-1}, from 700 to 600 cm^{-1}, respectively.

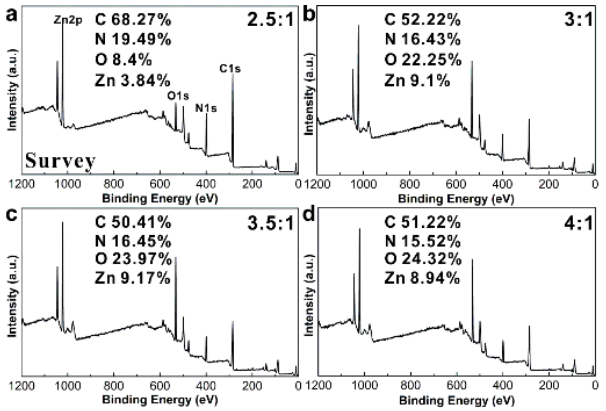

Fig. 5. XPS surface spectra of ZIF-8 films synthesized with different mole ratios of reactants, (a) 2.5:1, (b) 3:1, (c) 3.5:1 and (d) 4:1.

The XPS characterizations were further carried out to investigate the surface structures of ZIF-8 films. The survey spectra of ZIF-8 films with low crystallinity (x=2.5, 3, 3.5 and 4) (Fig. 5) and with high crystallinity (x=5, 6 and 8) (Fig. S11a-c) all show the presence of Zn, C, N, and O elements (Element H can't be detected due to its low binding energy.). And the relative content of C and N elements gradually is reduced, O content is gradually increased with the increase of mole ratios, indicating that ZIF-8 films synthesized with low mole ratios show lower coordination degree between zinc and ligand imidazole, thus having a high Hmim content relative to zinc comparing with those ZIF-8 films synthesized at high mole ratios. And acetic acid molecules in ZIF-8 composite films synthesized with low mole ratios may occupy the adsorption site of the ZIF-8 competing with oxygen species.[31] In this sense, C and N content is relatively high and O content is low. It can also be seen that Zn content of ZIF-8 film synthesized with the mole ratio of 2.5:1 is less than other samples due to the presence of more guest molecules CH_3COOH and the ligand is relatively deficient. The XPS spectra of Zn2p (Fig. S12 and Fig. S11d-f) are composed of two peaks centered at ~1022 eV and ~1045 eV, consistent with the binding energies of Zn $2p^{3/2}$ and $2p^{1/2}$, respectively.[32] This indicates that Zn^{2+} is present in the samples.

The XPS spectra of C 1s demonstrate three different types of peaks in all ZIF-8 samples (Fig. S13 and Fig. S11g-i), mainly corresponding to C-sp^3, C=C and C=N in 2-methylimidazole ring with binding energy values of ~284.8, ~285.7, ~288.3 eV, respectively,[12,33,34] which may be some signals from acetic acid molecules in ZIF-8 films with low mole ratios.[35] And the N 1s peaks shown in Fig. 6 and Fig. S11j-l at ~398.9 eV and ~400.6 eV confirm the presence of C=N-C and N-H bonds, respectively,[12,36] indicating that there are N sites (N-H) uncoordinated with zinc ions in all ZIF-8 films, which can serve as binding sites of guest molecules. The difference is that N-H existing in ZIF-8 films synthesized with low mole ratios is caused by the lower coordination degree due to relatively low deprotonation degree of Hmim in $Zn(Hmim)_n^{2+}$, while ZIF-8 films synthesized with high mole ratios are terminated at N-H because of excess ligand. In this sense, the relative intensity of N-H increases with the mole ratio increasing due to higher coordination degree and more terminal ligands. The O 1s signal (Fig. S14) of ZIF-8 films synthesized with low mole ratios probably comes from the capturing CH_3COOH molecules, CH_3OH and absorbed CO_2 and H_2O on the surface. However, the O 1s (Fig.S11m-o) of ZIF-8 films synthesized with high mole ratios mainly comes from absorbed CO_2 and H_2O.[37]

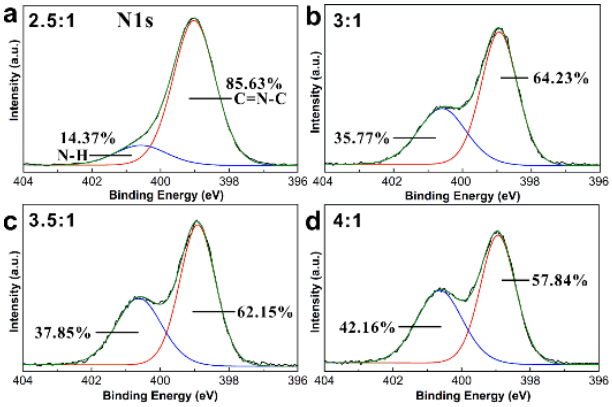

Fig. 6. XPS high resolution N1s spectra of ZIF-8 films synthesized with different mole ratios of reactants, (a) 2.5:1, (b) 3:1, (c) 3.5:1 and (d) 4:1.

3.2. Formation mechanism of ZIF-8 film with CH_3COOH molecules

In our works, the whole reaction system includes $Zn(CH_3COO)_2{\cdot}2H_2O$, Hmim and CH_3OH. $Zn(CH_3COO)_2{\cdot}2H_2O$ was used as zinc source, CH_3OH was solvent and Hmim served as organic linkers to coordinate with Zn^{2+} for the formation of ZIF-8. The specific forming process mainly includes the following two steps: nucleation and growth of ZIF-8. The possible formation mechanism of ZIF-8 films with CH_3COOH molecules is shown in Fig. 7. The reactions occur in ZIF-8 sols system as following equations:[27]

$$Hmim + H_2O \leftrightarrow H_2mim^+ + OH^- \quad (1)$$

$$Zn(CH_3COO)_2 + 2H_2O \leftrightarrow Zn(OH)_2 + 2CH_3COOH \quad (2)$$

$$Zn^{2+} + n\ Hmim \rightarrow Zn(Hmim)_n^{2+} \quad (3)$$

$$Zn(Hmim)_n^{2+} + Hmim \rightarrow Zn(Hmim)_{n-1}(mim)^+ + H_2mim^+ \quad (4)$$

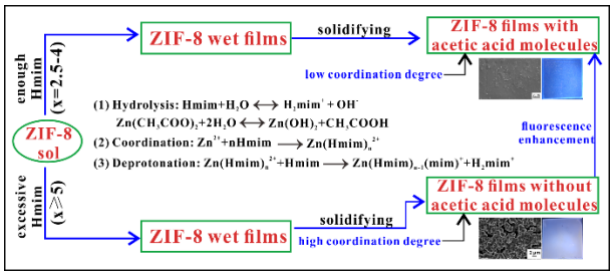

Fig. 7 Possible schematic illustration for the formation mechanism of ZIF-8 films with CH_3COOH molecules.

Herein, reactants $Zn(CH_3COO)_2{\cdot}2H_2O$ and Hmim organic ligands hydrolyse in methanol to reach equilibrium before the coordination of Zn^{2+} with Hmim, respectively. Hmim competes with water to bind with the zinc ions released from the zinc source in the reaction system. Since Hmim has a higher basicity (pK_a[Hmim]=14.2) possessing higher electron density, it is easy to coordinate with transition-metal ions.[37,38] In this sense, Hmim would coordinate with Zn^{2+} to form $Zn(Hmim)_n^{2+}$ ($1\le n\le 4$), which would make the pH of reaction system drop quickly because of breaking of the equilibrium equation of Hmim toward the left-hand. And the Hmim is sufficient comparing with the stoichiometric ratio to form ZIF-8 ($Zn(mim)_2$, mole ratio of ligand to zinc salt is 2:1), a part of Hmim would consume H^+ from $Zn(Hmim)_n^{2+}$ through hydrolysis to achieve the purpose of $Zn(Hmim)_n^{2+}$ deprotonation, and finally forming the ZIF-8 nucleuses.[27] Additionally, under the condition of keeping zinc acetate concentration constant, there is a hydrolysis equilibrium about CH_3COO^-. After the organic ligand Hmim coordinates with Zn^{2+}, it will facilitate the hydrolysis of CH_3COO^- to form CH_3COOH due to dropping of pH of the sol. Finally, CH_3COOH and Hmim coexist in the sol.

Acetic acid belongs to a weak acid which can participate in the regulation of the pH of the whole reaction system. However, there is a difference in ZIF-8 sol with different mole ratios. As a Lewis base, Hmim is not only involved in the coordination with zinc ions and the deprotonation of $Zn(Hmim)_n^{2+}$, but also regulates the pH of ZIF-8 sols, so it is important to control the content of Hmim for preparation of ZIF-8 films. When the mole ratio is between 2.5:1 and 4:1 in the sol, the pH of the whole sol measured was ~8, which is weakly alkaline. This indicates that the coordination amount between ligand and zinc ions is relatively insufficient due to the large amount of Hmim used to neutralize acid. Moreover, the formation of $Zn(Hmim)_n^{2+}$ complexes deprotonates slowly or even can't be deprotonation because of the weak alkalinity of the whole sol system, resulting in low coordination degree between Zn^{2+} and Hmim and eventually forming transparent ZIF-8 sol through further growth. As for the ZIF-8 sols synthesized with high mole ratios ($x\ge5$) , the pH of sol was up to ~10 due to the increasing of Hmim ligands. This suggests that the ligand Hmim used for coordination with zinc ions and deprotonation will increase after neutralizing a certain amount of acetic acid, which is favourable for the nucleation and growth of ZIF-8. Therefore, the formed sol is relatively transparent (5:1 and 6:1) or non-transparent (8:1) because of the relatively big particles of ZIF-8 comparing with the sols of low mole ratios. When a small amount of acetic acid was added into the ZIF-8 sol prepared by the molar ratio of 8:1, the sol gradually changed from white suspension into colourless and transparent sol accompanied with exothermic phenomenon. Furthermore, some acetic acid is also added to the ZIF-8 sol synthesized with a mole ratio of 2.5:1. The results suggest that it is hard to form ZF-8 due to the limitation of the deprotonation process of $Zn(Hmim)_n^{2+}$ and inhibition of the nucleation and growth of ZIF-8. This indicates that the addition of acetic acid can regulate the pH of the sol system and reduce the amount of ligand Hmim involved in the coordination with zinc ions, which would slow down the complex deprotonation process of $Zn(Hmim)_n^{2+}$.

The wet ZIF-8 film obtained by spin-coating of ZIF-8 sols will undergo secondary growth during solidifying. The solidifying condition was 100 °C for 10 h in air atmosphere. Due to the presence of small molecules acetic acid and Hmim for regulating the pH of the sol system, the wet film will have not only the removal of methanol and water, but the volatilization of acetic acid and Hmim molecules during the solidifying process, which will change the pH of the wet film and cause the secondary growth of ZIF-8. Under the condition of low mole ratios, due to the slow deprotonation process of $Zn(Hmim)_n^{2+}$ resulting in the presence of uncoordinated N active sites as shown in Fig. 6, and Hmim used for $Zn(Hmim)_n^{2+}$ deprotonation is not enough. Therefore, some acetic acid molecules in the films may be captured by ZIF-8 framework through forming hydrogen bonds interaction with the N active sites in ZIF-8 structure before they are removed during the secondary growth of ZIF-8, and finally ZIF-8 composite film with CH_3COOH molecules were obtained at low mole ratios. However, the relative content of Hmim participated in deprotonation of $Zn(Hmim)_n^{2+}$ is excessive under the condition of high mole ratios, and acetic acid molecules in ZIF-8 wet films evaporate before they can be interacted with ZIF-8. Additionally, the residual imidazole ligands and acetic acid will be removed during solidifying. In this sense, pure ZIF-8 films with high crystallization are synthesized. In summary, ZIF-8 films containing acetic acid molecules were successfully synthesized at low mole ratios and pure ZIF-8 films can be obtained at high mole ratios.

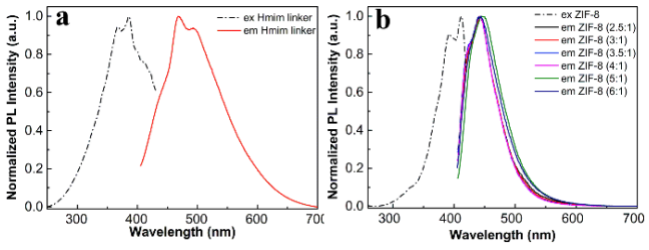

Fig. 8. The excitation spectra (dotted lines) and emission spectra (full lines, λex=386 nm) of the Hmim linker (a) and the ZIF-8 film samples at different molar ratios of reactants (b).

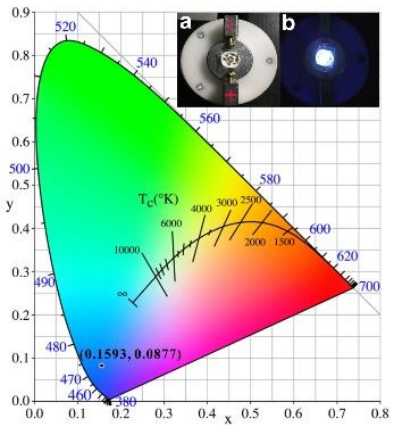

Fig. 9 CIE chromaticity coordinates of the ZIF-8 film (3:1) with blue-light emission (λ_{ex}=367 nm). The inset is photographs of fabricated blue LED (365 nm excitation) chip at on state (a) and off state (b).

3.3. Luminescent properties

It is interesting that ZIF-8 films synthesized with low mole ratios show higher transmittance and stronger fluorescence (365 nm excitation) comparing with the pure ZIF-8 films synthesized with high mole ratios. This may be relative to the guest molecules CH_3COOH in ZIF-8 films. Therefore, UV-vis absorption spectra of ZIF-8 films synthesized with different mole ratios were measured (the result of the ZIF-8 film synthesized with mole ratio of 8:1 was not shown because of poor film-forming quality). As shown in Fig. S15, all ZIF-8 films exhibit a sharp absorption edge at ~240 nm, which originates from the Hmim ligand of ZIF-8,[40] and the band gap estimated for ZIF-8 is approximately 5.17 eV according to the enlarged absorption spectra, which is consistent with the reported values (4.9 eV and 5.1 eV).[41,42] Furthermore, all ZIF-8 samples ranging from 250 to 500 nm show broad absorption bands with different intensities. The excitation and emission spectra of ZIF-8 films and Hmim powder are exhibited in Fig. 8. At ambient temperature, the emission spectrum of Hmim ligand shows a main peak at 468 nm upon excitation of 386 nm, presenting a broad PL emission at the range from 400 nm to 600 nm, and this emission may be attributed to the π^*-π transition of Hmim.[43,44] After Hmim linkers coordinate with metal Zn ions to form ZIF-8, a blue fluorescence with a peak at ~443 nm is observed for all ZIF-8 samples under the excitation wavelength at 386 nm, which blue shift about 25 nm comparing with the Hmim powder. According to previous reports, the metal organic frameworks with transition-metal ions without unpaired electrons (particularly with d^{10} metal centres) may exhibit liker-based emissive properties, so the blue emission of all the ZIF-8 films is caused by Hmim linker-based.[40,45,46] However, the photoluminescence mechanism is still unclear.

Additionally, it can also be seen that there is no obvious effect on the emission peak of the fluorescence of ZIF-8 itself after ZIF-8 captures acetic acid molecules. However, PLQY of the ZIF-8 film has been significantly improved, and the results are shown in Fig. S16 and Table S2. The PLQY of ZIF-8 films for the mole ratios of 8:1, 6:1, 5:1, 4:1, 3.5:1, 3:1, 2.5:1 are 4.03%, 16.50%, 16.42%, 44.36%, 46.96%, 44.42%, 54.42%, respectively. This indicates that the ZIF-8 films synthesized with the mole ratio of 2.5:1 contains the most guest molecules CH_3COOH and shows the highest PLQY upon the excitation at 365 nm, which is also higher than PLQY of ZIF-8 samples in other previous works shown in Table 1. Additionally, the fluorescence lifetime decay spectra of ZIF-8 films synthesized with different mole ratios were measured and results are shown in Fig.S17 and Table S3. It can be seen that the average fluorescence lifetime of all ZIF-8 films synthesized with different mole ratios are almost the same, which is about 2.7 ns. This suggests that introduction of guest molecule (acetic acid) into the ZIF-8 film puts little effect on the fluorescence lifetime of ZIF-8 itself. However, it can improve the PLQY of ZIF-8, this may be related to the structure and fluorescence lifetime distributions in ZIF-8 films.[47,48] Herein, a blue light-emitting diode (blue LED) was fabricated based on 365 nm GaAsP ultraviolet LED chip and a ZIF-8 film (3:1) with the size of 8×8 mm shown in Fig. 9, with Commission Internationale de l'Éclairage (CIE) coordinates of (0.1593, 0.0877) showing stable blue emission. In this sense, the ZIF-8 film by capturing guest molecules (CH_3COOH) is potential for light-emission applications.

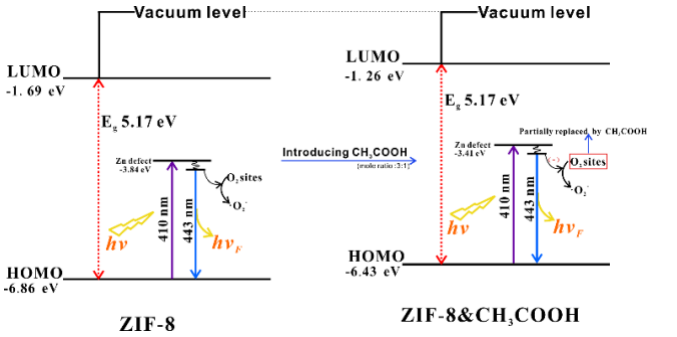

Fig. 10 Schematic diagram of fluorescence enhancement of the ZIF-8 composite film by capturing acetic acid molecules.

Table 1 Comparison of ZIF-8 materials on Photoluminescence quantum yield.

ZIF-8 materials	Excitation wavelength	Emission peak	Absolute PLQY	reference
ZIF-8 crystalline	396 nm	444 nm, 472 nm	3.6 %	[15]
ZIF-8 powder	365 nm	490 nm	4.73%	[18]
core-shell MOFs nanoparticles Tbx@ZIF-8 NPs	304 nm	543 nm	13.4%	[14]
core-shell MOFs nanoparticles Tbx@ZIF-8@F-ZIF-90@PDA NPs	304 nm	543 nm	19.1%	[14]
ZIF-8 film with guest molecules CH_3COOH	365 nm	443 nm	54.42%	In this work

3.4. The possible fluorescence enhancement mechanism about ZIF-8 composite film

The possible fluorescence enhancement mechanism about ZIF-8 film by capturing acetic acid molecules is displayed in Fig. 10, and band levels are calculated according to UV-vis spectra (Fig. 15), PL spectra (Fig. 8) and UPS results (Fig. S18). It can be seen that all ZIF-8 films including the pure ZIF-8 film (6:1) show same blue emission at 386 nm excitation in Fig. 8, this indicates that the blue emission is based on the ZIF-8 structure. The terminology of HOMO-LUMO gap can be utilized to describe the luminescence of the ZIF-8.[31,49] Electrons transfer from the highest occupied molecular orbital (HOMO) to the lowest unoccupied molecular orbital (LUMO) in ZIF-8 when giving a certain amount of energy. The LUMO is mainly localized on the zinc ions, and the HOMO is mainly contributed by N 2p in linkers. Additionally, Michael Chin et.al.[50] have studied not only the LUMOs of ZIF-8 with different coordination models between Zn ions and Hmim ligands ($Zn(mim)_4$, $Zn(mim)_3$, $Zn(mim)_2$ and Zn(mim), but also the LUMOs of ZIF-8 with a variety of surface groups including hydrogenocarbonate (CO_3H-), hydroxide(-OH) and secondary amine (-NH-). According to the work, $Zn(mim)_3$, $Zn(mim)_2$ and Zn(mim) models can exist at open Zn sites providing orbitals for electron transfer and the NH groups can act as Brønsted acid sites to donate protons which don't change the LUMO of ZIF-8. In our work, it can be seen from XPS data of the ZIF-8 films except for the ZIF-8 film synthesized with the mole ratio of 2.5:1 due to uneasy deprotonation of $Zn(Hmim)_n^{2+}$ ($1 \le n \le 4$) complexes and more amorphous disordered structure, the surfaces are Zn-rich of relative to imidazole in comparison to the expected stoichiometry of ZIF-8 ($C_8H_{10}N_4Zn$), suggesting the presence of terminations of Zn.[51] In this sense, there may be some open Zn sites in the films which may have an impact on the LUMO of ZIF-8. And N1s data of all ZIF-8 films also show the presence of the N-H groups. According to the aforementioned band gap of ZIF-8 (E_g=5.17 eV), 365 nm light can provide photon energy ~3.40 eV, which is not enough to trigger the electron in ZIF-8. Hence, the Zn defects may exist in ZIF-8 films from open Zn sites so that they can be triggered by lower photon energy.

In general, HOMO has the capacity to donate electrons and thus can be used to estimate the negative ionisation potential, and LUMO stands for electron acceptor estimating to the negative of electron affinity.[52] As seen in Fig. 10, both HOMO and LUMO energies of the ZIF-8&CH_3COOH after capturing acetic acid are increased by 0.43 eV compared with that of the ZIF-8. This indicates lower ionisation potential (HOMO) and higher electron affinity (LUMO), in which it is easier to donate and accept electron due to introduction of acetic acid molecules. In this sense, CH_3COOH can serve as an electron-donor in the ZIF-8 composite films containing small molecules CH_3COOH.[52] Upon excitation by UV light, the electrons which are easier to trigger in acetic acid molecules may be transferred to the ZIF-8, finally leading to fluorescence enhancement. On the other hand, the presence of acetic acid molecules also occupies the adsorption site of oxygen species, resulting in relative reduction of the electrons in the excited state captured by the oxygen species,[31,48] and eventually the ZIF-8 film containing CH_3COOH shows higher fluorescence. Since the presence of acetic acid affects the electron distribution and oxygen species content of ZIF-8, the acetic acid content is closely related to the PLQY of the ZIF-8 film.

4. Conclusions

In short, we reported a facile strategy to prepare a ZIF-8 film with enhanced blue fluorescent performance by a sol-gel method. Using zinc acetate dihydrate as zinc sources, the blue fluorescence of ZIF-8 have been enhanced by introducing small molecules CH_3COOH in ZIF-8. The relative content of CH_3COOH and the coordinating degree between Zn^{2+} and ligands can be regulated by the mole ratios, so that the optical performance of ZIF-8 films is controlled. The ZIF-8 film synthesized with a mole ratio of 2.5:1 possesses low coordination degree and contains small molecules ~20%. Furthermore, the PLQY (blue emission due to existence of open Zn sites) of the ZIF-8 film is up to 54.42% under 365 nm excitation, compared with 16.5% of the pure ZIF-8 film. This may be relevant to the electron transfer between small molecules CH_3COOH and ZIF-8, and reduction of oxygen adsorption sites. In this sense, the ZIF-8 film with enhanced fluorescence has a great potential in the light-emitting applications.

Conflicts of interest

There are no conflicts to declare.

Acknowledgements

This work was supported by the National Natural Science Foundation of China (Grant No. 51772229), "111" project (No. B18038), the National Key R&D Program of China (No. 2017YFE0192600), the provincial Key R&D program of Hubei (No. 2020BAB061), Open Research Fund Program of Science and Technology on Aerospace Chemical Power Laboratory (No. STACPL220191B02), Open Foundation of the State Key Laboratory of Silicate Materials for Architectures at WUT (No. SYSJJ2020-04) and State Key Laboratory of Materials Processing and Die & Mould Technology (No. P2021-010), Huazhong University of Science and Technology. We also thank the Analytical and Testing Center of WUT for the help with carrying out XRD, TEM, and FESEM analyses.

References

1 Y. Yan, J. Gong, J. Chen, Z. Zeng, W. Huang, K. Pu, J. Liu and P. Chen, *Adv. Mater.*, 2019, 31, 1808283.
2 D. Chen and X. Chen, J. Mater. Chem. C, 2019, 7(6): 1413-1446.
3 Z. Song, J. Zhao and Q. Liu, Inorg. Chem. Front., 2019, 6(11): 2969-3011.
4 M. D. Smith, B. A. Connor and H. I. Karunadasa, Chem. Rev., 2019, 119(5): 3104-3139.
5 L. Su, X. Fan, T. Yin, H. Wang, Y. Li, J. Li, H. Zhang and H. Xie, Adv. Optical Mater., 2019, 1900978.
6 Z. Zhuang and D. Liu, Nano-Micro Lett., 2020, 12(1): 1-32.

7 H. Q. Yin and X. B. Yin, Acc. Chem. Res. 2020, 53, 485-495.
8 K. S. Park, Z. Ni, A. P. ôté, J. Y. Choi, R. Huang, F. J. Uribe-Romo, H. K. Chae, M. O'Keeffe and O. M. Yaghi, PNAS, 2006, 103(27), 10186-10191.
9 J. Yang, Y. B. Zhang, Q. Liu, C. A. Trickett, E. Gutierrez-Puebla, M. Á. Monge, H. Cong, A. Aldossary, H. Deng and O. M. Yaghi, J. Am. Chem. Soc. 2017, 139, 6448-6455.
10 B. Chen, Z. Yang, Y. Zhu and Y. Xia, J. Mater. Chem. A, 2014, 2, 16811-16831.
11 X. Lin, G. Gao, L. Zheng, Y. Chi and G. Chen, Anal. Chem., 2014, 86(2): 1223-1228.
12 Y. Wang, B. Wang, H. Shi, C. Zhang, C. Tao and J. Li, Inorg. Chem. Front., 2018, 5, 2739-2745.
13 T. Han, H. Bai, Y.Liu and J. Ma, J. Solid State Chem., 2019, 269: 588-593.
14 D. Mo, Z. Wang, K. Sun, X. Xie, J. Zhang and K. Cai, J. Mater. Chem. C, 2020, 8, 11110-11118.
15 Chang Liu and Bing Yan, Eur. J. Inorg. Chem. 2015, 279-287.
16 X. Hu, X. Liu, X. Zhang, H. Chai and Y. Huang, Biosens. Bioelectron, 2018, 105, 65-70.
17 W. Chen, S. Kong, J. Wang, L. Du, W. Cai and C. Wu, RSC Adv., 2019, 9, 3734-3739.
18 X. Yang and D. Yan, Chem. Commun., 2017, 53(11).
19 X. Chen, X. Jiang, C. Yin, B. Zhang and Q. Zhang, J. Hazard. Mater. 2019, 367, 194-204.
20 W. Xue, Q. Zhou, F. Li, B. S. Ondon, J. Power Sources 2019, 423, 9-17.
21 M. U. A. Prathap and S. Gunasekaran, Adv. Sustainable Syst. 2018, 1800053, 1-9.
22 J.Troyano, A. Carné-Sánchez, C. Avci, I. Imaz and D. Maspoch, Chem. Soc. Rev., 2019, 48, 5534-5546.
23 J. Cravillon, C. A. Schröder, H. Bux, A. Rothkirch, J. Caro and M. Wiebcke, CrystEngComm, 2012, 14, 492-498.
24 H. Kaur, G. C. Mohanta, V. Gupta, D. Kukkar and S. Tyagi, J. Drug Deliv. Sci. Tec., 2017, 41, 106-112.
25 O. Abuzalat, D. Wong, S. S. Park and S. Kim, Nanoscale, 2020, 12, 13523.
26 Y. Hu, H. Kazemian, S. Rohani, Y. Huang and Y. Song, Chem. Commun., 2011, 47, 12694-12696.
27 M. Jian, B. Liu, R. Liu, J. Qu, H Wang and X. Zhang, RSC Adv., 2015, 5, 48433-48441.
28 X. Q. Li, J. J. Luo, L. Deng, F. H. Ma, and M.H. Yang, Anal. Chem. 2020, 92, 7114-7122.
29 Z. Wang, D. Sun, X. He, Beijing: Petroleum Industry Press, 1982, 263-268.
30 L. Yang and H. Lu, Chin. J. Chem. 2012, 30, 1040-1044.
31 H. Jing, C. Wang, Y. Zhang, P. Wang and R. Li, Rsc Advances, 2014, 4 (97): 54454-54462.
32 N. Li, L. Zhou, X. Jin, G. Owens and Z. Chen, J. Hazard. Mater. 2019, 366: 563-572.
33 Gi Xue, Q. Dai and S. Jiang, J. Am. Chem. Soc., 1988, 110 (8), 2393-2395.
34 I. J. Villar-Garcia, E. F. Smith, A. W. Taylor, F. Qiu, K. R. J. Lovelock, R. G. Jones and P. Licence, Phys. Chem. Chem. Phys., 2011, 13, 2797-2808.
35 K. Kishi and Y. Ehara, Surf. Sci., 1986, 176, 567-577.
36 C. Hu, Y. Huang, A. Chang and M. Nomura, J. Colloid Interface Sci., 2019, 553, 372-381.
37 S. Liu, F. Chen, S. Li, X. Peng and Y. Xiong, Appl. Catal. B: Environ, 2017, 211,1-10.
38 J. P. Zhang, Y. B. Zhang, J. B. Lin and X. M. Chen, Chem. Rev. 2012, 112, 1001-1033.
39 J. Cravillon, R. Nayuk, S. Springer, A. Feldhoff, K. Huber and M. Wiebcke, Chem. Mater. 2011, 23, 2130-2141.
40 C.-W. Tsai, R.E. Kroon, H.C. Swart, J.J. Terblans, R.A. Harris, J. Lumin., 2019, 207, 454-459.
41 F. Wang, Z. S. Liu, H.Yang, Y. x. Tan and J. Zhang, Angew. Chem. 2011, 123, 470-473.
42 S. Panneri, M. Thomas, P. Ganguly, B. N. Nair, A. P. Mohamed, K. G. K. Warrier and U. S. Hareesh, Catal. Sci. Technol., 2017, 7, 2118-2128.
43 S. Liu, Z. Xiang, Z. Hu, X. Zheng and D. Cao, J. Mater. Chem., 2011, 21, 6649-6653.
44 G. Zhao, H. Wu, R. Feng, D. Wang, P. Xu, H. Wang, Z. Guo and Q. Chen, ACS Omega 2018, 3, 9790-9797.
45 J. Zou, L. Li, S. You, K. Chen, X. Dong, Y. Chen and J. Cui, Cryst. Growth Des. 2018, 18, 3997-4003.
46 C. Liu and B. Yan, Photochem. Photobiol. Sci., 2015, 14(9): 1644-1650.
47 K. Rautaniemi, Elina Vuorimaa-Laukkanen, C. J. Strachan and T. Laaksonen, Mol. Pharmaceutics 2018, 15, 1964-1971.
48 X.F. Liu, L. Zou, C. Yang, W. Zhao, X.Y. Li, B. Sun, C. X. Hu, Y. Yu, Q. Wang, Q. Zhao and H. L. Zhang, ACS Appl. Mater. Interfaces 2020, 12, 43073−43082.
49 M. A. Nasalevich, M. van der Veen, F. Kapteijn and J. Gascon, CrystEngComm, 2014, 16, 4919–4926.
50 M. Chin, C. Cisneros, S. M. Araiza, K. M. Vargas, K. M. Ishihara and F. Tian, RSC Adv., 2018, 8, 26987-26997.
51 F. Tian, A. M. Cerro, A. M. Mosier, H. K. Wayment-Steele, R. S. Shine, A. Park, E. R. Webster, L. E. Johnson, M. S. Johal and L. Benz, J. Phys. Chem. C, 2014, 118, 14449-14456.
52 M. A. Hossain, J. Jewaratnam, A. Ramalingam, J.N. Sahu and P. Ganesan, Fuel, 2018, 212, 49-60.

